Semiconductor superlattices: A tool for terahertz acoustics

Agnès Huynh, Bernard Perrin, A Lemaître

Semiconductor superlattices: a tool for terahertz acoustics

A. Huynh[a,*], B. Perrin[b], A. Lemaître[c]

[a] *Sorbonne Universités, UPMC Univ Paris 06, UMR 7588, Institut des Nanosciences de Paris, F-75005, Paris, France*
[b] *CNRS, UMR 7588, Institut des Nanosciences de Paris, F-75005, Paris, France*
[c] *CNRS, UPR 20, Laboratoire de Photonique et de Nanostructures Route de Nozay, 91460 Marcoussis, France*

Abstract

The properties of optical to acoustic transduction of semiconductor superlattices have been explored for several years in the sub terahertz frequency range. Using femtosecond laser pulses focused on these structures, acoustic modes are excited with a frequency related to the periodicity of the structure stacking. We have shown that these acoustic waves can be extracted and can propagate in the underlying substrate. We study superlattices ability to be quasi monochromatic generators. On the other hand, superlattices have been found to be very sensitive and selective detectors. We present a set of experimental results concerning the generation, propagation over large distances and detection of acoustic waves at high frequencies, up to the challenging 1 terahertz by picosecond ultrasonics experiments in transmission geometry.

1. introduction

The progress in miniaturization and the technological development to create multilayers stackings drive the scale of interest in the nanometer range. In parallel, the availability of monochromatic phonon sources at ultrahigh frequencies with their wavelength in the nanometer range would be of great interest to study the elastic properties of such nanostructures, to image buried nanostructures and achieve high resolution acoustic microscopy, or to allow the conception of acousto-optic devices working at the picosecond time scale[1, 2, 3, 4]. Classical piezoelectric transducers deliver coherent acoustic waves up to only a few Gigahertz. Acoustic phonons with higher frequencies, up to a few THz are generated with heat-pulse techniques. Indeed, acoustic phonons are the main contributors in the heat transport and at low temperature, their mean free path becomes macroscopic. Propagation of terahertz phonons by heat-pulse techniques has been extensively studied since the pioneering work of Von Gutfeld[5]. Several devices based on incoherent phonons and heat transfer have been proposed and analysed, as thermal diodes[6, 7, 8, 9, 10, 11], transistors[12] or logic gates[13]. These devices rely on broadband incoherent phonons which response rapidity is limited by heat transfer and then are restricted to low-frequency applications. Coherent phonon in the sub THz range represent a realistic alternative to rapidly modulate electronic or optical properties. Moreover phonon spectroscopy would benefit from the availability of a coherent source of monochromatic phonons. There was a breakthrough with the use of the pump probe techniques with femtosecond lasers[14], leading to the birth of the picosecond ultrasonic technique. In a conventional picosecond ultrasonic experiment, a sound pulse is generated if a pump pulse is absorbed in a metallic film deposited at the surface of the sample. Its frequency spectrum can extend up to a few hundreds GHz. When an acoustic echo returns to the surface, the small change $\Delta R(\mathrm{t})$ in the optical reflectivity of the sample is measured with a time-delayed probe light pulse. Thin metallic films or semiconductor quantum wells[15] allow to reach the sub THz range but remain broadband transducers, with a high frequency cut-off limited by the layer thickness or the optical absorption length. To obtain an acoustic field of a given wavelength, one needs to specifically design types of structures such as periodic multilayers structures. Superlattices (SLs) exhibit zone folding of the acoustic branches within the Brillouin zone due to the artificial periodicity of the elastic properties along the growth direction. This leads to the appearance of several phonon modes in the acoustic range, with a frequency $f \neq 0$ and a wave vector $q \approx 0$, to which light can couple. This is the way to excite zone-folded acoustic modes at higher frequencies, up to the THz range. Vibrational properties of such structures have been studied by Raman[16, 17, 18, 19] and phonon transmission spectroscopy[20], giving a detailed understanding at thermal equilibrium[21]. Laser ultrasonics is a powerful technique well adapted to the study of SLs, as sub THz phonon dynamics can be measured by femtosecond laser pulses, which are short enough in comparison with the period of the acoustic waves. These ultrafast experiments showed that high frequency modes can be coherently excited or controlled in various multilayers such as semiconductor SLs, around 100 GHz in Si/Ge[21] or GaAs/AlGaAs[22] SLs, at 0.5/0.9 THz[23, 24, 25] in GaAs/AlAs SLs. In metallic multilayers localized surface modes were demonstrated in addition of folded modes, at a frequency of

*Corresponding author
Email address: agnes.huynh@insp.jussieu.fr (A. Huynh)

0.7 THz[26], 1.2 THz[27], or even 2.25 THz in Co/Cu[28], as in Mo/Si multilayers[29, 30]. But few works have been devoted to SLs as generators and to the acoustic waves leaking from the SLs. The experimental demonstration on the propagation through a substrate of acoustic pulses optically excited in SLs was first reported using an energy detector with a superconducting bolometer deposited on the other side of the sample[31]. A subsequent experiment using a second SL as an acoustic filter gave support to the coherence of the emitted phonons[32] though leaving the spectral width of the generated phonons unknown. In this paper we describe several experimental configurations to study generation, propagation over macroscopic distances and subsequent detection of coherent sub terahertz phonons. After a description of the SLs we use for this purpose in section 2, we present the experimental procedure and the different configurations used to study SLs as generators or detectors (section 3). The following sections will be devoted to some experimental results about the light-to-sound transduction properties of SLs.

2. Superlattices

2.1. Principle

The formal similarity between the equations describing light and sound propagation has been the basis for the conception and demonstration of 1D[20, 33], 2D[34] and 3D[35] phononic crystals in which the acoustic impedance is artificially modulated as the refractive index is in photonic crystals.

Thus, semiconductor superlattices extensively used as distributed Bragg mirrors for photons can also act as high reflectance phonon mirrors in the GHz-THz range[20, 36]. Thanks to the development of growth processes, it is possible to obtain large stackings of layers with a period of a few nanometers, and with interface fluctuations of one atomic monolayer. These conditions are required to design mirrors in the THz range. A SL consists of a periodic stacking of a bilayer, here GaAs and AlAs. The periodic modulation of elastic properties leads to a modification of the phonon dispersion, which exhibits a folding of the phonon branches into a brillouin zone of dimension π/d, where d is the thickness period. Due to impedance mismatch between the two components, frequency gaps open at the zone center and at zone boundaries, at wave vector $q = n\pi/d$, where n is integer. The sound propagation through this periodic stacking is a complex process of interferences between waves which reflect at each interfaces. For specific frequencies, corresponding to these gaps, destructive interferences in transmission take place, so that the multilayer acts as a mirror, which reflectivity increases with the number of periods. GaAs and AlAs acoustic impedances are closely matched (the acoustic impedance contrast $\frac{|Z_1-Z_2|}{\sqrt{Z_1 Z_2}}$ on which depends the appearance of gaps, is only 20%), which means that gaps are not very large and a few tens of periods are needed.

Another mismatch between the two constituants is the optical absorption. For the light wavelength used here (700-820 nm), light is only absorbed into GaAs layers. Different processes can be involved in coherent phonon generation in condensed matter : photothermal generation, deformation potential, piezoelectric and electrostriction effects. For any of these processes the two layers of a period exhibit different properties which means that a strain field modulation is expected with a dominant period equal to the SL period. Hence the modes $q = 0$ can be easily generated by light absorption in these systems.

On the other hand, when an acoustic wave goes through a SL, a transient modulation of the SL optical properties occurs, resulting in a transient change of the SL reflection. SLs can then detect phonons via photoelastic detection. Furthermore, a condition of phase matching is required. Indeed, a SL is a semi-transparent media where the interaction of light with coherent phonons is strongly enhanced at the acoustic wave vector $q = 2k$ in backscattering configuration, where k is the electromagnetic wave vector.

The filtering, generation and detection properties of GaAs/AlAs superlattices are extensively studied throughout this paper.

2.2. Samples

Samples were grown by molecular beam epitaxy on a double-side-polished [001]-oriented GaAs substrate. They consist of n periods of ($3\lambda_1/4$, $\lambda_2/4$) GaAs/AlAs bilayers, where $\lambda_i = c_i/f$ with c_i the sound velocity of longitudinal acoustic phonons in each material, and f the frequency corresponding to the center of the first zone-center gap. This condition fulfilled by the thicknesses of the two materials maximizes the width of this gap. We use for c_i the values 4.78 and 5.66 nm.ps^{-1} for the velocity at low temperature in GaAs and AlAs respectively, deduced from fitting processes. We studied 4 samples where the SL thickness is about 1 μm. The SL period was chosen so that the first zone-center gap falls at a frequency of 100, 200, 400 and 600 GHz. We label the samples S100, to S600, with respectively 20 40 80 and 120 periods. On the rear of the substrate, an aluminum film was deposited. For the need of one configuration, aluminum films were deposited on both sides of sample S100. The aluminum has the advantage to have a small acoustic mismatch with GaAs.

Another type of samples was studied, with two SLs on both sides of the GaAs substrate. A first SL was grown as the previous ones. During the second SL growth, the rotation of the substrate wafer was suppressed in order to obtain a gradient in the thicknesses of all layers, which we estimate to be of the order of 20% by X-ray and pump and probe measurements (cf. section 7). 3 samples, labeled DS400, DS800, DS1 were designed to work at different frequencies, 0.4, 0.8 and 1 THz. A summary of all samples are presented in the table 1, where the indicated values for thicknesses have been measured by X-ray technique.

Sample	first zone center gap (THz)	thickness GaAs/AlAs (nm)	number of periods
S100	0.095	35.9/14.8	20
S200	0.197	17.1/7.5	40
S400	0.395	8.6/3.9	80
S600	0.587	5.6/2.7	120
DS400	0.393	8.9/3.5	100
DS700	0.715	4.7/1.8	175
DS800	0.787	4.3/1.7	200
DS1	1.008	1.4/3.5	250

Table 1: Characteristics of the samples. S100 to S600 are constituted by one SL grown on a GaAs substrate. DS400 to DS1 contain two SLs on each side of the substrate, one of which presents a thickness gradient of all layers. The characteristics done here correspond to the uniform SL, the other SL having thicknesses of the same order.

3. Experimental procedure

3.1. Configurations in acoustic transmission

Interferometric pump-probe experiments were performed, using a femtosecond mode-locked Ti:Sapphire laser providing 80 fs pulses (200 fs pulses incoming on the sample), with a 80 MHz repetition rate. The pump is modulated at 1 MHz to allow synchronous detection through a lock-in amplifier. The probe beam is time-delayed by a mechanical delay line, able to reach a delay of 11.5 ns. The transient changes of the complex optical reflectivity $\Delta R/R$ are measured by a Sagnac interferometer[37]. This allows access to the real and imaginary parts of $\Delta r/r$ where r is the reflectivity of the amplitude of the field. Both beams are focused onto 60 μm wide spot with a typical energy of 0.1 to a few nJ/pulse for the pump. Our originality is to focus the pump beam on one side of the sample while the probe beam is impinging on the other side, which requires a more demanding alignment in order to have both beams face to face, but it is completely free of non-vibrational contributions (electronic or thermal relaxation), in contrast to classical experiments with pump and probe focused on the same side of the sample.

Concerning samples with one SL, two configurations are possible. In the configuration which we will call "detection", the pump beam, focused on the metallic film, is absorbed over a short penetration length, and leads to the generation of an acoustic pulse[38]. The aluminum thickness (30nm) is optimized to minimize direct absorption by the substrate while being small enough to get a pulse frequency range extending up to 250 GHz. This acoustic pulse propagates through the thick GaAs substrate (330 to 372 μm) before reaching the SL where it is detected through the change of reflectivity: this is the first echo. To have negligible attenuation during propagation, we cool down the sample to 15 K. If the initial strain is large enough, during propagation on such large distances, non-linear distortion of the initial acoustic pulse occurs, which could give rise to solitons[39, 40] and high frequencies conversion. Furthermore, due to the total reflection on the sample free surfaces, the generated pulse travels back and forth several times through the substrate, giving rise to echoes arriving at time delays $(2p+1)T$ where T is the transit time (69 to 78 ns, depending on the substrate thickness). T being larger than the time interval $T_{\text{laser}} \approx 12.5$ ns between laser pulses, echoes are detected modulo T_{laser}; for sake of simplicity, and also because attenuation can become important, we only analyse the first echo. In the reverse configuration, called "generation", we test the ability of the SL to generate and emit phonons by focusing the pump beam directly on the SL; after propagation through the substrate, emitted phonons are detected by the time-delayed probe pulse reflected by the aluminum film. For the same reasons we will focus on the first echo.

3.2. Asynchronous optical sampling (ASOPS)

A variation of the experimental set-up has also been used (*cf.* section 6.3). The idea is to be able to vary the wavelength of the probe or the pump beam, independently. This is possible by using an asynchronous optical sampling[41, 42, 43], where two mode-locked fs lasers are used, linked by a fixed repetition rate difference $f_p - f_s$, of the order of several kHz. Due to the repetition rate detuning, probe pulses are incoming on the sample with a relative time delay which varies linearly. The sampling process repeats itself when the cumulative delay equals the period of the pump laser (T_{laser}), which is scanned in a duration equal to $f_p \frac{f_s}{f_p - f_s}$. Typically $f_p - f_s = 5$ kHz, that implies a fast measurement (0.2 ms for one scan). Measurements are similar but avoid the use of a mechanical delay line and a lock-in detection. A good signal to noise ratio is obtained faster. However, the time resolution is limited to 2.5 ps (0.4 THz), for acoustic signal lasting more than a few nanoseconds, due to limitations of the lasers repetition rate stabilization.

4. Charaterization of superlattices

A first experiment performed with available metallic transducers was to measure the acoustic transmission of a SL. As Aluminum films are efficient up to 200 GHz, the sample we chose was S100. Aluminum films were deposited on both sides of the sample. The experiment scheme is sketched on figure 1, where is schematically shown the acoustic strain launched through the substrate from the metallic film on the rear of the substrate, and its possible distorsion during propagation for the largest acoustic strains; this pulse goes through the SL and is detected by the Al film deposited on the SL. The figure 1 shows the real part of the signal where one can see the arrival of the short pulse at $t_0 \sim 76.5$ ns, the time needed for going through the substrate, followed by fast oscillations, and 1700 ps later, a weaker signal. With the combination of

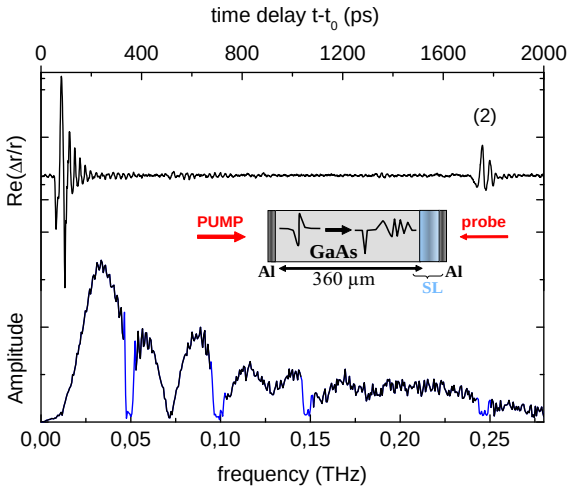

Figure 1: Transmission experiment as it is sketched with pump and probe beams focused on opposite sides of the sample. Up, time-resolved reflectivity (real part); (2) denotes the signal corresponding to the second echo, and $t_0 \sim 76.5\,\mathrm{ns}$. Bottom, FT amplitudes of the time derivative of the corresponding signal on the time interval [0, 1700 ps]. The frequency range of the phonon stop bands are emphasized in blue.

the value of t_0 and the laser repetition rate, this last signal appears to be the detection of the second echo, *i. e.* the acoustic pulse which has been reflected on the interfaces with air and made an additional round trip.

To see the modifications induced by the SL in the frequency spectrum, Fourier transform of the time derivative (FT) of the signal is performed on the time interval [0, 1700 ps]. Including the second echo in the FT modifies a little the low frequency range ($< 50\,\mathrm{GHz}$). In the spectrum shown figure 1, the transmission vanishes over some frequency ranges, emphasized in blue, which correspond to the stop bands which exist every 50 GHz. Because the building blocks of the SL period are $(3\lambda/4,\ \lambda/4)$, the second gap in the zone center is closed, which is confirmed experimentally. The third gap at the Brillouin zone edge can be seen at 250 GHz. To confirm these observations, and confirm the stop bands spectral positions, the pump intensity was varied. Indeed, at that relatively high pump intensity, the acoustic pulse impinging on the SL has likely undergone non-linear propagation; that explains that the slowly varying envelope is distorded, that dips appear due to frequency up-conversion and that the spectrum can go up to nearly 0.3 THz. If the excitation intensity is lowered, the envelope changes as it can be seen in figure 2(a), leaving the stop-bands identical.

To reproduce qualitatively these spectral features, one needs to calculate the strain impinging on the SL. For this purpose, we have to take into account first, thin layer effects in the phonon generation spectrum in the aluminum layer and secondly, non-linear propagation in the thick GaAs substrate.

Several papers have studied theoretically the generation of strain pulses by laser ultrasonics techniques [44, 45, 46].

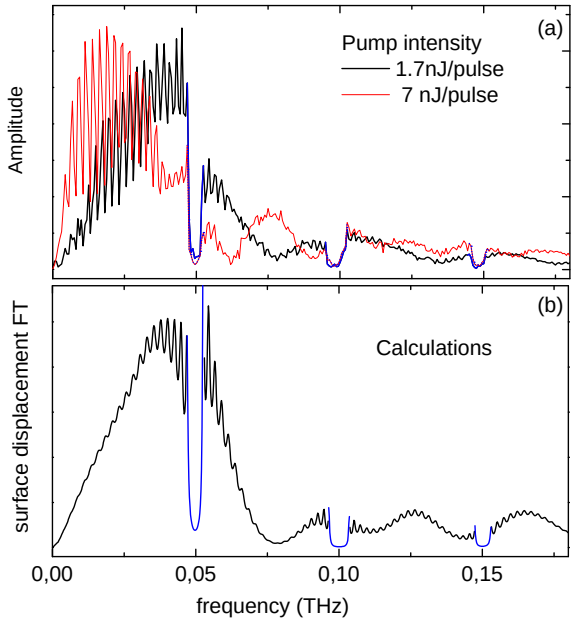

Figure 2: Transmission experiment: (a) FT amplitudes of the time derivative of the transient reflectivity signal (imaginary part) for two pump intensities; (b) calculation corresponding to the spectra obtained at 1.7 nJ/pulse

The initial strain in aluminum is well approximated by

$$\eta(z,t) = \eta_0 \mathrm{sgn}(z - v_{\mathrm{Al}} t)\, e^{-\alpha_{\mathrm{Al}}\,|z - v_{\mathrm{Al}} t|}$$

where $v_{\mathrm{Al}} = 6.33\,\mathrm{nm/ps}$, and $\alpha_{\mathrm{Al}} = 6.9\,\mathrm{nm}^{-1}$ are the sound velocity and the optical absorption coefficient in the aluminum film. This initial strain can be large enough to undergo a non-linear propagation through the substrate. Sound dispersion, sound absorption and non-linear effects, are described by a 1D Korteweg-De Vries (KDV) equation[39, 47] as far as diffraction is negligible:

$$\partial_t \eta = \epsilon \partial_z^2 \eta - \gamma \partial_z^3 \eta - \frac{C_{\mathrm{nl}}}{2 v_0 \rho_{GaAs}} \eta \partial_z \eta \qquad (1)$$

where ϵ, γ and C_{nl} are the acoustic attenuation, dispersion, and nonlinearity, and v_0 and ρ_{GaAs}, the sound velocity and mass density of GaAs. Sound absorption is negligible in the frequency range we consider, at low temperature. We solve numerically this equation with the help of a composite Runge-Kutta algorithm[48]. The initial amplitude of the strain is the adjustable parameter. We took in the literature the values of the acoustic dispersion ($\gamma = 7.4\,10^{-3}$ $\mathrm{nm}^3 ps^{-1}$) and the acoustic nonlinearity ($C_{\mathrm{nl}} = -2.661^{-4}$ $\mathrm{fg.nm}^{-1}.\mathrm{ps}^{-2}$).

Once the strain impinging on the SL is obtained, the following step is the calculation of the acoustic field in the multilayers (SL+Al film) which is performed with a standard transfer matrix formalism[28]. The acoustic field is calculated in each layer. We have used the layer thicknesses independently determined by X-Ray diffraction, corrected by a factor of -0.5% to adjust the frequency stop bands. The displacement of the sample surface is then easily obtained and it is normalized with the relevant incoming acoustic spectrum impinging on the SL.

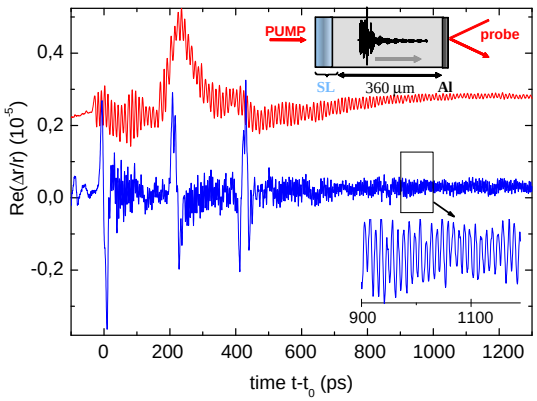

Figure 3: Generation configuration as indicated by the sketch (with a calculated strain wave packet propagating inside the substrate). Time-resolved reflectivity (real part) for: up (in red) sample S100 at 2.8 nJ/pulse and a laser wavelength $\lambda = 752$ nm; and bottom (in blue) sample S200 at 7.5 nJ/pulse and a laser wavelength $\lambda = 735$ nm; the inset shows an expanded region, where oscillations can be seen with a period of 5 ps.

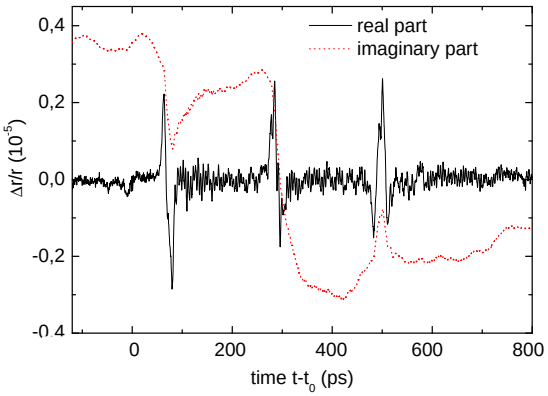

Figure 4: In the generation configuration, comparison of the imaginary (dotted line) and the real part (solid line) of the time-resolved reflectivity sample S200 at 7.5 nJ/pulse and a laser wavelength $\lambda = 780$ nm.

Generally speaking, the change of reflectivity of the probe field amplitude in an opaque film with a thickness of d can be written as the sum of the term due to surface displacement and the one due to the photoelastic effect[49, 14, 27, 44]:

$$\frac{\Delta r}{r} = ik_0 2n_0 u_0(t) + ik_0 \frac{4n}{1-n^2}\frac{\partial n}{\partial \eta}\int_0^d dz\ \eta(z,t)\, e^{2ink_0 z} \tag{2}$$

where k_0, n_0, u_0 are the wave vector of the probe light in the air, the air index, the displacement of the free surface, and n, η and $\frac{\partial n}{\partial \eta}$ the optical index of the film, the strain and the photoelastic constant. The imaginary part of the experimental signal is 3 to 5 times larger than its real part[40]. We then assume in a simple approach that the imaginary part of the reflectivity is mainly due to surface displacement.

The figure 2(b) shows the calculated FT displacement and the overall correspondence with the transmission structure at 1.7 nJ/pulse is remarkable, including the observation of three gaps around 0.05, 0.1 and 0.15 THz (emphasized in blue).

These experiments validate the concept of phononic mirror. Thus, SLs have been used as mirrors to form phonon nanocavities[50, 51] or microcavities to obtain a strong optomechanical coupling[52]. Acoustic amplification was realized in doped GaAs/AlAs SLs and recently a saser, for sound amplification by the stimulated (acoustic phonons) radiation was demonstrated, in a device including a SL gain medium and GaAs/AlAs SLs acoustic mirrors[53].

5. Generation by superlattices

5.1. Experimental results

Once SL filtering properties were demonstrated, we were interested to use them as active devices[54]. In this section we study them as phonon generators, by directly focusing the pump pulse on the SL. A broadband phonon detector is placed on the other side of the substrate, to detect phonons which have escaped from the SL in the underlying substrate. The experimental configuration is reminded in the inset of figure 3, where is represented inside the substrate the wave packet generated by a SL, calculated in the theoretical frame previously described. We used again a 30 nm aluminum film. The change of reflectivity (real part) on the metallic film is shown on figure 3, measured on samples S100 and S200. Both signals present fast oscillations that last for a long time, 2 to 3 ns, in contrast with short acoustic pulses generated by metallic films. First of all, let's focus on the three short variations appearing at the beginning of the signal, which remind us of acoustic pulses. These features appear also in the imaginary part of $\Delta R/R$ as jumps and peaks, as it can be seen in figure 4. They are less visible for sample S100 probably because the laser wavelength is not optimized (see § 5.3). These peaks are separated by a duration of approximately 200 ps, corresponding to the transit time through the SL. Indeed, when the light is absorbed along the whole SL and reaches the rear interface, acoustic pulses are generated at the interfaces substrate/SL and SL/air: (1) two pulses at the interface with the substrate, one launched through the substrate, which is the first detected peak, another one launched through the SL and coming back after reflection with the interface with air, hence delayed by twice the transit time; (2) a pulse at the interface with air, corresponding to the second detected peak, as it has propagated through the SL.

As expected as the light penetrates through the whole SL, and due to different optical and acoustic properties, an acoustic strain modulated at the superlattice period is created. Generation of coherent phonons is expected in a narrow frequency range. It occurs at the wave vector $q = 0$ for an infinite SL, that is near the gaps in the Brillouin zone center. For symmetry considerations, only the lower energy mode around $q = 0$ will be excited. With a SL constituted of m periods of thickness d, the acoustic resonances occur at frequencies corresponding to wave

vector $q = n\,\pi/md$, with $n \in \mathbb{N}$ and $\frac{n}{m} \notin \mathbb{N}$ in the extended Brillouin zone of the related infinite structure. The main peak frequency is down shifted relatively to $q = 0$ mode, is broadened and small resonances appear. The superimposed fast oscillations in the signal for S100 and S200 have a frequency of respectively 94 and 197 GHz for samples S100 and S200 respectively. These frequencies correspond to the lower band edge as expected, slightly downshifted, in the first gap, as it can be seen in the comparison of the dispersion curve and the FT amplitude of the signal (figure 5a). The excitation of the mode in the second gap, which is closed for these SLs, is less efficient. For S100, one can see a weak doublet, corresponding to $q \approx 0$, with an amplitude comparable to Bragg peaks appearing around the first gap.

In front configuration, phonon generation and detection occur simultaneously on the same SL, a triplet is usually observed, corresponding to two modes at $q = 2k$ and one at $q = 0$. In contrast this experiment clearly shows that there is no emphasized excitation at $q = 2k$.

5.2. Comparison with calculations

Coherent acoustic phonons generation mechanisms have been discussed in literature[14, 55], and most of works concerning the ultrafast optical excitation of acoustic phonons have shown the contributions of the thermoelastic and deformation potential processes, with a domination of the latter process[56]. Coherent acoustic phonons can be efficiently excited by the piezoelectric effect, as it has been demontrated in strained multiple quantum wells[57, 58] or by electrostriction[59]. It is not necessary to describe the generation mechanism, as for all these mechanisms, a localized strain is created proportional to the electric field intensity. Following the same framework of the transfer matrix method, exposed in section 4, we can easily obtain the displacement B_s launched in the underlying substrate. Here, as the pump pulse penetrates through the SL, the electromagnetic field is calculated in each layer and the interaction of the SL with the incoming light is assumed to leave a stress proportional to the local electromagnetic field energy in GaAs layers only. Indeed, at these light energies, AlAs is transparent. We neglect here optical reflection on the interface between the SL and the substrate. The sound wave propagation equation is solved in each layer, taking into account this stress source term and boundary conditions to obtain the acoustic field everywhere. Here, we estimate that the propagation was linear. Indeed, 100 GHz or 200 GHz oscillations were measured with an amplitude of 10^{-4} in $\Delta r/r$ at quite high pump intensities (about 7.5 nJ/pulse), and we will see that the strain incident on the Al film at these frequencies could be estimated to less than 10^{-6}. At such strain value, only dispersion occurs and the acoustic pulse spectrum is unchanged when impinging on the SL. $\Delta r/r$ was then calculated, including contributions of the surface displacement and photoelastic effects in aluminum. The displacement

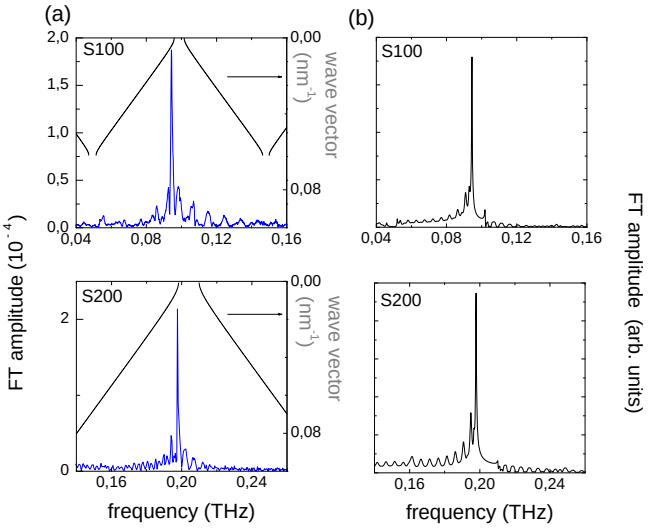

Figure 5: In the generation configuration, (a) FT amplitudes of the real part of the transient reflectivity for samples S100 and S200 corresponding to the temporal signals shown fig. 3, compared to the dispersion curve and (b) the corresponding calculations.

of the film is thus given by:

$$A_f = B_s \times \frac{Z_s}{Z_s \cos(qd) - iZ \sin(qd)} \tag{3}$$

$$\frac{\Delta r}{r} = A_f \frac{8i\pi}{\lambda} \left(1 + \frac{p_{Al} n}{1 - n^2} \times \frac{2q^2}{4k^2 - q^2}\right) \tag{4}$$

where Z and Z_s are the film and sustrate impedances, q and k the wave vectors of phonon and probe light, $n = 0.86 + 5.32\,i$ the index of Aluminum film measured by ellipsometry, and $p_{Al} = -28 + 15\,i$[60], the photoelastic coefficient of aluminum. B_s is the displacement which propagates in the substrate.

We obtain an excellent agreement with the experimental data, as it can be seen in figure 5. The figure 6 shows that this simple model reproduces well the difference of amplitude between real and imaginary part, and a more important content at low frequencies for the imaginary part. However, small discrepancies remain in the low frequency side, and in the temporal domain (fig. 3 in blue), refinements are needed to reproduce the importance of the three peaks at the beginning of the signal relatively to oscillations with the $q = 0$ mode frequency.

Compared to the previous section where only the displacement spectrum was calculated, the complete calculations do not bring more informations on details of the measured spectrum. What is interesting is that they give the possibility to estimate the SL performances as phonon generators. By comparing the amplitude obtained at 100 and 200 GHz with a quite high pump intensity (7.5 nJ/pulse) (10^{-3} and 2×10^{-4} respectively) to the calculated amplitude of $\mathrm{Re}(\Delta R/R)$, one can deduce the initial displacement and consequently the strain generated by the SL; we obtain $3.5{\times}10^{-8}$ at 100 GHz and 2.5×10^{-8} at 200 GHz. At these pump intensities, we checked that saturation already occurs, we can conclude that in our experimental

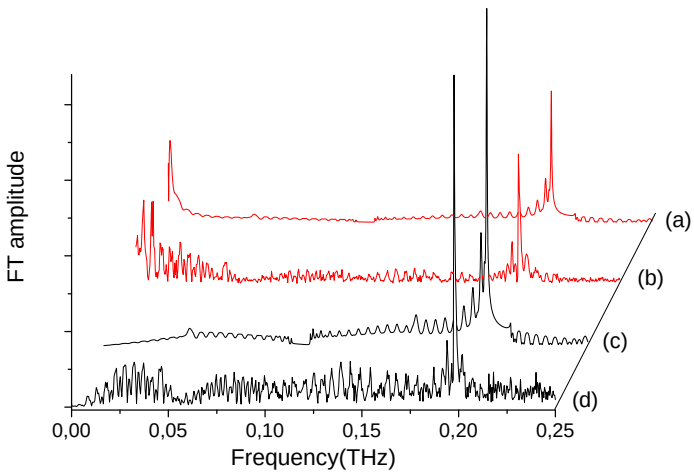

Figure 6: In the generation configuration, comparison in the frequency domain of the transient reflectivity for sample S200, the imaginary part, measured (b) and calculated (a) and the real part, measured (d) and calculated (c) at 7.5 nJ/pulse and a laser wavelength $\lambda = 735$ nm.

conditions, GaAs/AlAs SLs, with the [001] orientation (no piezoeletric effects), generate quasi monochromatic acoustic pulses with a strain amplitude which will not overcome 10^{-7}, but which last a few nanoseconds.

We performed the same experiment at higher frequencies. For the sample S400, the signal has a very weak component at 393 GHz, with an amplitude of 1.2×10^{-5} as it is shown on figure 10. Compared to the dispersion curve, this corresponds to the q=0 mode, as expected. We reach the limitations of the metallic film as a detector, whose sensitivity decreases for high frequencies.

5.3. Influence of the wavelength excitation

A few work has been done about the efficiency of generation by SLs[23, 24, 61]. As the dominant mechanism in semiconductor systems, the deformation potential should depend on the excitation wavelength. These works consist of pump and probe experiments around the band gap, but since pump and probe energies change simultaneously the generation and detection processes are intimately correlated. In [61] it was possible to decouple the effect of varying the energy of the optical excitation as phonons were detected via a bolometer: the integrated amplitude of the longitudinal acoustic phonon strongly increases when the SL becomes absorbant. Above the gap, a smaller peak is also observed, corresponding to a resonant absorption process. Here to measure the efficiency of SLs as quasi monochromatic phonon sources, we vary the wavelength laser up to 813 nm and take benefit from the fact that detection efficiency in aluminum films is not very sensitive to wavelength between 750 and 820 nm ([62]). Recently we checked that performing this experiment while the probe

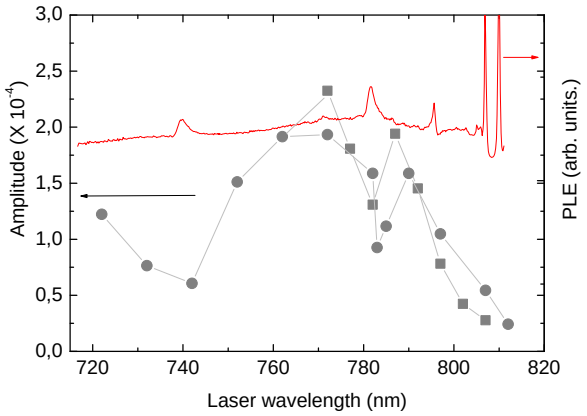

Figure 7: In the generation configuration, amplitude of the generated mode at $q = 0$ at the frequency of 197.6 GHz in the FT of the imaginary part of transient reflectivity for sample S200 at 7.5 nJ/pulse.

wavelength is set to a constant (with ASOPS) gives similar variations. Results are shown figure 7 and indicate that the amplitude varies by a factor of 10 on the range [720;812]. To find a correlation with the electronic transitions estimated at 813 nm, we measure the excitation of the photoluminescence (PLE) at 5 K, plotted on the same graph which reflects the absorption in so far as relaxation processes are not too slow. Peaks at 780 nm, and the two ones around 815 nm are indentified as the excitonic transitions (E2HH2, E1LH1 and E1HH1 respectively). Another transition appears at 740 nm. They have a clear influence on the amplitude of the $q = 0$ mode, visible even if the pump bandwidth is about 10 nm and broadens peaks. A resonant behavior at the crossing of a transition is observed, at least for transitions at 740 and 780 nm, in agreement with previously cited measurements. In particular, above E1HH1 transition, $\lambda > 820$ nm, the signal strongly decreases.

6. Detection by superlattices

6.1. Selection rule and efficiency

The acoustic pulse coming from the substrate and entering in the SL causes a periodic modulation of the optical properties of the SL, resulting in a transient change of the probe reflectivity. One reason is the displacement of the surface and the many interfaces (rippling), due to the appearance of a strain, and another cause is the local modulation of the refractive index due to transient perturbation of the electronic distribution. The expression of the change of reflectivity given in equation 1 for an opaque film is modified for a SL as the strain is modulated and one needs to sum over the different layers; in an effective medium from the optical point of view, only the second term has to be modified, and becomes proportional to [28]:

$$\sum_p \frac{\partial \epsilon_p}{\partial \eta} \int_0^{d_p} dz\ \eta_p(z)\, e^{iq_p z}\, (a_p e^{ikz} + b_p e^{-ikz})^2 \qquad (5)$$

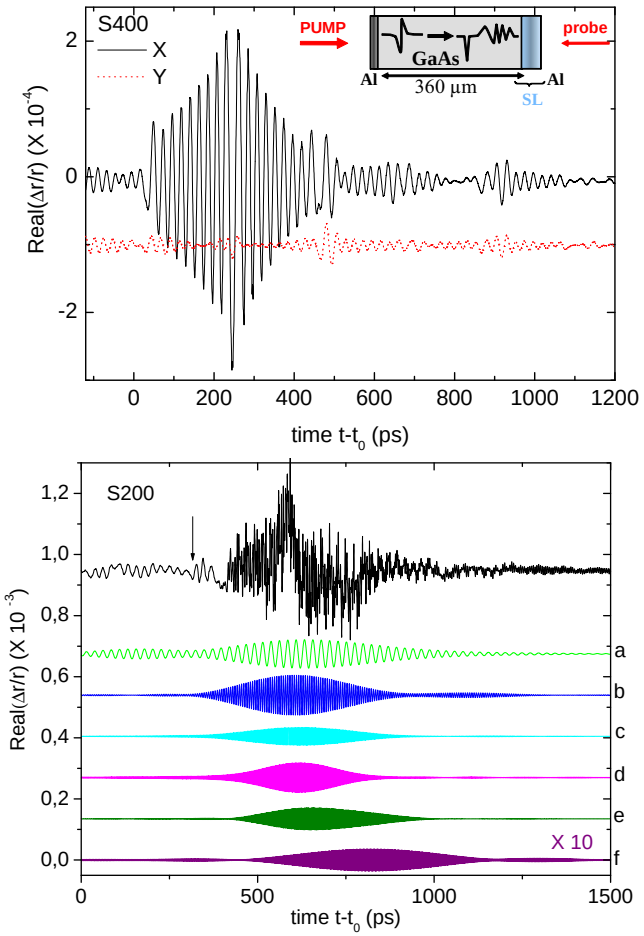

Figure 8: In the detection configuration, up, (see sketch in the inset), real part of the transient reflectivity for sample S400, at 3.5 nJ/pulse and a laser wavelength $\lambda = 779$ nm. The two channels of the lock-in detection are shown. $t_0 \approx 70.7$ ns. Bottom, real part of the transient reflectivity for sample S200, at 12.3 nJ/pulse and a laser wavelength $\lambda = 800$ nm. The arrow indicates the pulse arrival at the aluminum film, at the time $t_0 \sim 77.8$ ns. Below are shown the signal filtered around detected frequencies (a): 42 GHz, (b): 161 GHz, (c): 249 GHz, (d): 365 GHz, (e): 450 GHz, (f): 567 GHz.

where p is relative to the p^{th} layer, q_p is the corresponding acoustic phonon wave vector, and k the effective electromagnetic wave vector in the SL. In particular, a_p is the amplitude of the probe electric field penetrating in the SL, b_p the one reflected by the interface substrate/SL, usually neglected. In this case, in a sufficiently transparent medium for the probe, the interaction of coherent phonons with light is enhanced for acoustic wave vectors satisfying $q = 2k$. This reflects the phase matching in the exponential term. In particular the lowest possible detected frequency corresponds to the Brillouin oscillation, which is usually observed in semi-transparent bulk materials. It should be noted that finite size and light absorption cause the relaxation of these selection rules.

In the "detection configuration", we invert the role of SL and aluminum film compared to the "generation configuration" to measure the detection by a SL of an acoustic pulse produced by the film and having propagated through the substrate. The figure 8 shows two typical signals, one at low pump intensity on S400 (up) and another on S200 (bottom) where the pump intensity was increased enough to obtain nonlinearities during propagation. What is first observed is the Brillouin oscillations, visible tens of picoseconds before the beginning of both signals (indicated by an arrow for S200). They may come from the detection of the incoming pulse in the substrate. Indeed, due to the weak transparency of the SL, the probe light can reach the substrate and detect the acoustic pulse before the latter reaches the SL. Other contributions to these initial Brillouin oscillations are distant echoes detected at the same delays. Indeed, due to the repetition rate of the laser pulses, echoes are folded back into a 12.5 ns time window and distant echoes, whose frequency content has been reduced to low frequencies, can arrive at the same delays. In figure 8 up, distant echoes are visible on both lock-in channels at 500 and 900 ps, whereas the lock-in phase has been adjusted to detect the first echo on X channel only. Then the signal increase and decrease correspond to the acoustic pulse entering the SL and after reflection on the free surface, going back to the substrate. The time between the maximum and the beginning (or the end) of the signal corresponds to the time needed to cross the SL (≈ 200 ps). The signal in the linear regime is symmetrical with respect to the time when the pulse is reflected (figure 8, up) but not anymore when the pump intensity increases; indeed, at this quite high pump intensity, non-linear propagation occurs and extends the impinging spectrum on the SL. High frequencies appear and travel more slowly, resulting in a weak signal distorsion and appearance of fast oscillations in addition to preponderant Brillouin oscillations. In this case, the frequency content of these fast oscillations is shown on figure 9 and is composed of several frequencies which verify the selection rule $q = 2k$, as it can be seen by comparing the spectrum with the dispersion curve. High frequencies can be detected up to nearly 0.9 THz. Filtering the temporal signal at the largest spectral components, one can notice a shift of the arrival of each filtered echo, due to dispersion. However, this shift should not reflect the delay accumulated during propagation on the whole thickness of the substrate, as nonlinearities occur as far as the acoustic pulse propagates. However, this happens at the very beginning of the propagation. Calculations based on KDV equation (eq. 1) show that after a propagation on 20-30 μm (6% of the substrate thickness), a tail in the high frequency side (around 400-600 GHz) has already appeared in the strain spectrum with an important amplitude. This is consistent with the measured delays. If we expand the dispersion relation in the form $\omega = v_0\, q - \gamma q^3$ where $\gamma = 7.4 \times 10^{-3}$ nm^{3}ps^{-1} is the same dispersion coefficient in KDV equation, describing the dispersion at the lowest order, and v_0 the celerity for low frequency component, we deduce a group velocity $v_g = d\omega/dq = v_0 - 3\gamma q^2$. We then expect a relative delay (relatively to the travel

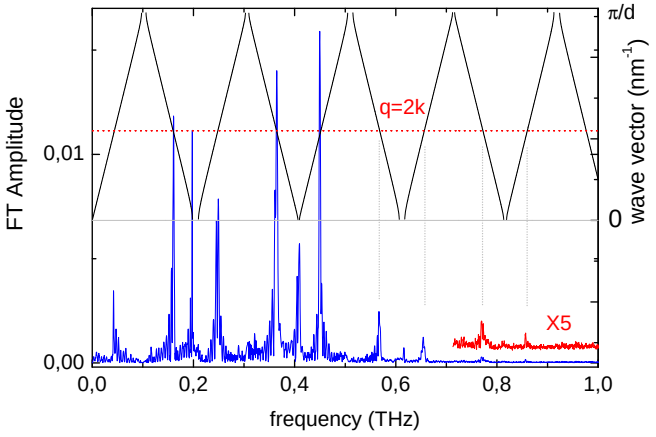

Figure 9: In the detection configuration, FT amplitude of the derivative of the transient reflectivity for sample S200, at 12.3 nJ/pulse and a laser wavelength $\lambda = 800$ nm, compared to the dispersion curve.

time t_0 through the sample at low frequency) of

$$\delta t/t_0 = 12\,\pi^2\gamma f^2/v_0^3 \qquad (6)$$

For instance for $f = 567$GHz (resp. 450 GHz), δt should reach the value of 180 ps (115 ps resp.), values in good agreement with experimental delays.

Another noticeable feature is the detection of $q = 0$ modes. Indeed, in the expression of $\Delta r/r$ (5), if the weak reflection on the interface SL/substrate is taken into account, the field which contributes is $a_p^2 e^{2ikz} + a_p\, b_p$, b_p being the reflected field amplitude. This results in the modified conservation rule: $q = 0$ and $q = 2k$. These features are visible for the other samples S400 and S600 (*cf.* figures 10(b) and 12). We will see in § 6.4 that we could benefit from that detection at $q = 0$ to generate and detect an acoustic pulse by the same SL.

Efficiency of detection

To be able to compare the efficiency of SLs as detectors, we perform the "detection" experimental configuration on samples where the detection takes place on an aluminum film instead of the SL, that is a substrate of GaAs with two Al film on both sides. We kept the same experimental conditions of pump intensity. The corresponding spectrum is compared to what is detected with S400 on figure 10b, and a factor of 500 was needed to obtain the same signal level. In addition, we show that SLs can detect acoustic pulses in the THz frequency range, with a very good sensitivity, whereas the Al film shows here its bandwidth limitations, being no more sensitive for frequencies higher than 400 GHz (at least in our experimental conditions of focalization).

At last, if we compare the three detectors S200, S400 and S600 which have the same global thickness but as a result, an increasing number of periods, the efficiency of detection increases with the latter, as it is illustrated in figure 11. The change of reflectivity, calculated in the spectral domain for each sample, is plotted keeping all parameters unchanged. We assume a gaussian spectrum in-

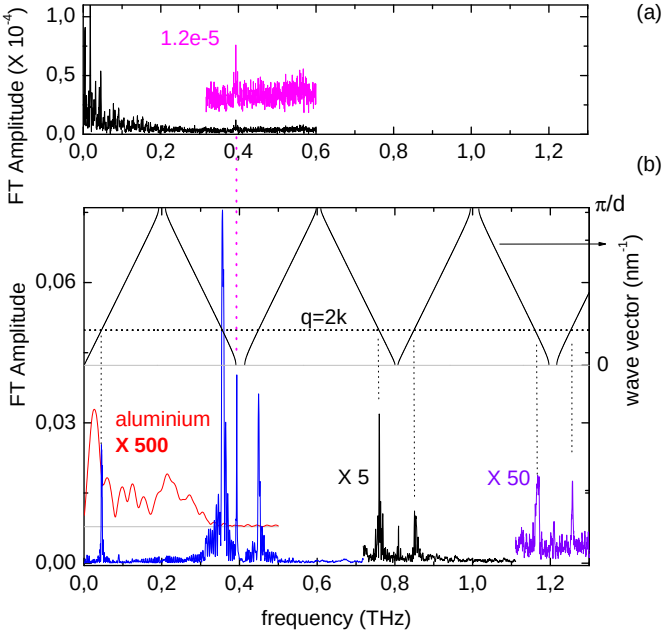

Figure 10: (a) In the generation configuration, FT amplitude of the Imaginary part of the derivative of the transient reflectivity for sample S400. (b) In the detection configuration, FT amplitude of the time derivative of the transient reflectivity superimposed on the dispersion curve, for sample S400, at 12 nJ/pulse and a laser wavelength $\lambda = 777$ nm and a detected spectrum obtained with an aluminum film in the same conditions.

cident on the SL, shown also for comparison. We see for instance that an acoustic signal with a 360 GHz component (respectively 550 GHz) is better detected by the SL having its first zone center gap near 400 GHz (respectively 600 GHz) than 200 GHz. As parameters are maintained constant for these calculations, we do not have included the important influence of the wavelength of the laser, a factor to take into account when one wants to use a SL as a detector (*cf.* § 6.3).

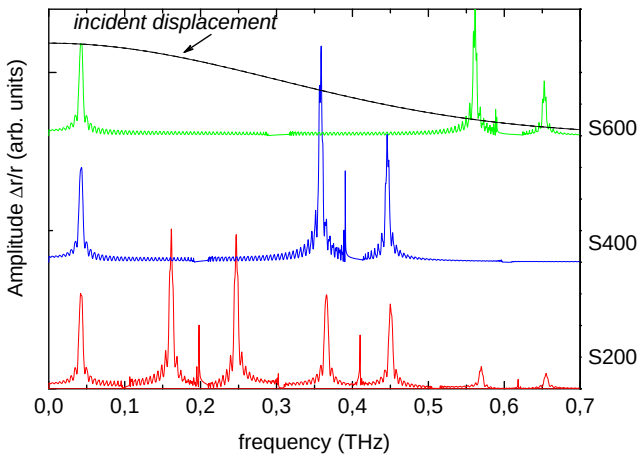

Figure 11: Amplitudes of the calculated change of reflectivity for sample S200, S400, and S600 in the spectral domain. For comparison, all parameters were kept constant when changing the number and thicknesses of the layers. Curves are shifted for clarity. The incident displacement used for the calculations is shown in dotted line.

6.2. Variation with pump intensity

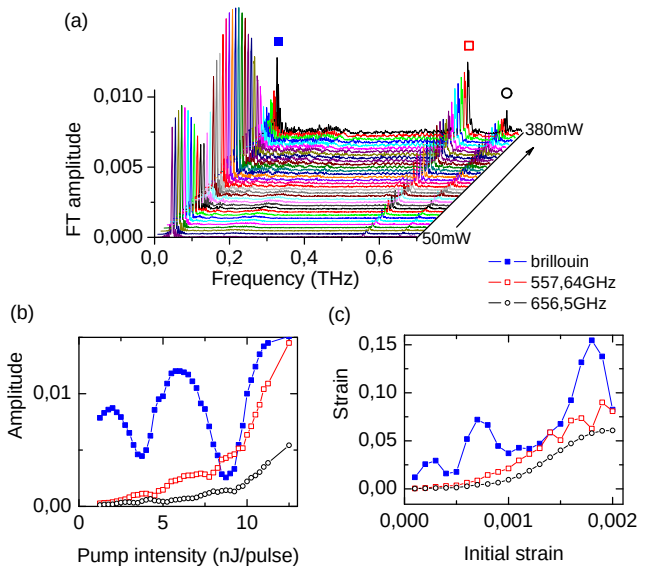

Figure 12: In the detection configuration, (a) FT amplitude of the derivative of the transient reflectivity for sample S400, for pump intensities varying from 50 to 380 mW by step of 5 mW and a laser wavelength $\lambda = 753$ nm. (b) The amplitude of the detected frequencies (marked with the square, the open square and circle), are reported as a function of pump intensity. (c) Relative amplitude of these components in the calculated strain spectrum impinging on the SL after non-linear propagation, as a function of the initial strain in the Al film.

When the pump intensity is varied on the metallic film, the non-linear character of acoustic wave propagation can be addressed by detecting the final strain by the SL. Instead of detecting a large spectrum as in previous works with metallic films in GaAs [39, 40] or Sapphire [63], the mechanism of detection will result in a selection of frequencies, but with a very good sensitivity, which allows to reach upper frequencies. The figure 12(a) shows a series of spectra obtained at increasing pump intensities by step of 10 mW, from 50 to 380 mW (1.25 to 9.5 nJ/pulse). This concerns sample S400, with expected frequencies verifying the selection rule $q = 2k$: $\nu_b = 47.3$ GHz (Brillouin), $\nu_1 = 470$ GHz and $\nu_2 = 655$ GHz (the $q = 0$ mode is very weak, visible at high pump intensity between ν_1 and ν_2). The Brillouin component is well detected even at low pump intensities, unlike ν_1 and ν_2 whose amplitude increases monotonously. ν_b amplitude, plotted on figure 12(b) oscillates. This can be understood if we consider the amplitude of the impinging strain on the SL, which is calculated by solving the KDV equation for an initial strain varying from 2×10^{-4} to 2×10^{-3}. The distorsion of the spectrum and frequency up-conversion result in oscillations in the strain amplitude at one given frequency in the low frequency range, whereas for high enough frequencies, the evolution is monotonous (*cf.* figure 12(c)). The variations of calculated strain amplitude at frequencies ν_b, ν_1, and ν_2 and the experimental amplitudes agree qualitatively. One notices a saturation arising in the detection efficiency around 5 nJ/pulse. Furthermore, the size of the probe beam spot is only slightly smaller than the pump beam spot, which has a gaussian profile of intensity. This implies that inside the probe beam, the measured displacements and photoelastic effects are due to a varying initial strain and are not homogenous, resulting in an average of non-linear effects. A necessary improvement would be to decrease the probe spot to measure a signal due only to a given initial strain.

6.3. Variation with wavelength

The laser wavelength has an important influence on the detection sensitivity. Indeed, the photoelastic coefficients play a dominant role in the detection function and even if their variation with laser energy is not very well known, they are expected to vary strongly in the vicinity of electronic transitions, as the complex index does. The passage of the acoustic wave in the SL results in a slight variation of the energy levels, and if the probe laser wavelength is tuned close to an electronic transition, which will vary, we expect a large variation of the relative reflectivity.

We perform a series of experiments where the probe wavelength varies while the pump wavelength and its intensity remain constant, at 750 nm and at about 8 nJ/pulse respectively. The latter is large enough to obtain a non-linear propagation, resulting in a broad spectrum impinging on the SLs S200 and S400. This is possible using the ASOPS set-up described in section 3.2 for sample S200. This works well for frequencies lower than 400 GHz, due to time resolution limitations of the set-up. To go further, for sample S400, we used the traditional set-up as generation by the aluminum film is not very sensitive for pump wavelength varying from 720 to 810 nm. The results are plotted in figure 13, where in (a) are compared the dispersion curve and the values of the frequencies we detect. The values verify the selection rule which slightly varies with probe wavelength. In the panel (b) we compare the variation of the FT amplitude at these frequencies with the photoluminescence (PL) and excitation of the photoluminescence (PLE), where can be recognised E1HH1 and E1LH1 transitions (790 and 780 nm for S400, 808 and 805 nm for S200). The detection shows a strong answer around these transitions, even if the convolution with the laser pulse (spectral width of 8 nm) makes difficult the precise interpretation. What is remarkable is that one obtains a gain of one order of magnitude in sensitivity, when the probe wavelength is closed to an electronic transition.

6.4. Round trip

As previously seen, the spectral response of phonon detection in SLs is modified when a sufficient refractive index difference allows an optical reflection at the interface between the substrate and the SL. Phonons with the wave vector $q = 0$ are weakly detected. Thus, in principle, a SL can generate phonons in the mode $q = 0$ and can also detect them. We exploit this idea by performing a straightforward experiment where a SL plays the role of generator

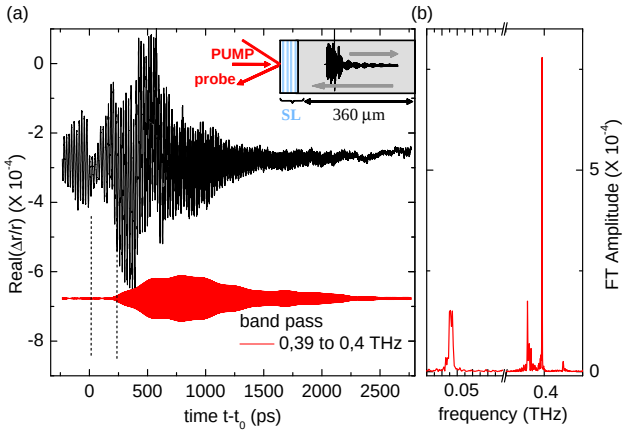

Figure 14: (a) In the "round-trip" experiment, (sketched in the inset) transient reflectivity for sample S400 in black, and band pass filter at $q = 0$ mode (0.395 THz) at a pump intensity of 1.8 nJ/pulse and a laser wavelength $\lambda = 778$ nm. Arrival times are indicated by dashed lines. (b) Corresponding FT of the derivative of the time trace. The peak amplitude amounts to $\sim 8\times10^{-4}$.

and detector. These measurements differ from what is usually done, that is studying the excited acoustic modes after excitation in the time range where the change of reflectivity is dominated by carriers dynamics. We were interested in the part of excited phonons at $q = 0$ which leaks from the SL, propagates through the substrate and comes back to be detected by the SL (*cf.* inset in figure 14). The difficulty is the weakness of the signal, which is dominated by the carrier dynamics (by 3 order of magnitude, as it will be seen). In addition, the time delay at which it should be detected is unknown as the thickness cannot be determined with a sufficient precision (an error of 1 μm implies a time delay difference of more than 400 ps). One can suspect a loss of high frequencies due to reflection on the back of the substrate, even polished [64]. Nevertheless we could measure the signal due to the acoustic pulse which has made one round trip in sample S400 (a propagation distance of about 700 μm), plotted on figure 14(a). The wavelength of the laser was adjusted to maximize the signal. Brillouin oscillations from distant echoes are mixed to the signal, and begin before the arrival of the acoustic pulse; the amplitude jump gives an accurate determination of t_0. By filtering the signal at $q = 0$ mode frequency (395 GHz), we obtain a symetrical signal with a shift of about 200 ps in the arrival time. That value is in agreement with the delay calculated from dispersion with a thickness of 346 μm, deduced from the measurement of two successive echoes.

The signal lasts long, about 2.25 ns. In comparison with the case of an acoustic pulse generated by a metallic film, with a duration of a few picoseconds, which was detected by the same SL, the signal duration is 4 times longer. Indeed, what is detected here is a wave packet lasting for nearly two nanoseconds (*cf.* figure 3).

In the frequency domain, $q = 0$ mode dominates by a factor 4 both Brillouin and $q = 2k$ modes. It can be surprising that these backscattering modes are detected as the SL generates a quasi-monochromatic wave at $q = 0$ mode. As it can be seen in the calculations (*cf.* figure 5(b)), we remind that the generated wave packets have a low frequency broad component and a peak at $q = 0$ whose basis is weak but broad enough in the low frequency side, so that an overlap exists with the mode $q = 2k$ at 356 GHz. These are finite size effects. That explains that, besides the main component at the $q = 0$ mode, the detected signal has also weak components at $q = 2k$.

7. Double SL samples

7.1. Principle and results

Associating a metallic film and a SL on opposite sides of the substrate, to use SLs as generators or detectors is very interesting to study the properties of SLs, taking benefit from the fact that aluminum films are phonon broad band emitters with a flat wavelength response. However this scheme suffers from spectral limitations of the metallic film. If one desires to reach higher frequencies, it is natural to think about associating two SLs on opposite sides of the substrate. The experimental configuration is sketched on figure 15(a). This scheme has been used with a separating 1-μm thick GaAs layer but optical coupling remains between the SLs and the role of each SL does not clearly appear [65, 66]. To that purpose, several samples have been grown as described in section 2.2. The thickness lateral gradient, introduced during the growth of one SL, gives a degree of freedom since the frequency of the $q = 0$ and $q = 2k$ modes varies with the position of the laser spot. It can be then possible to tune one detected frequency of the tapered SL to that of the $q = 0$ mode generated by the uniform SL, as shown on the dispersion curves on figure 15(b). The SL with a thickness gradient has slightly thinner layers for this configuration. It keeps the advantage of spatially separate the roles of generation and detection, and brings a selection on phonon frequency.

Let's focus on the signal obtained when the sample is moved relatively to the two beams. A large exploration has been done on sample DS1 resulting in the spectra shown on figure 15(c). A signal with a constant amplitude is found at the Brillouin frequency (not shown), whereas around the first gap in the zone center (≈ 1 THz), three peaks appear, corresponding to $q = 0$ mode and two relative to the selection rule $q = 2k$. For a peculiar position on the sample (at the scale origin on the figure) the $q = 0$ mode amplitude reaches a maximum, corresponding to the maximal overlap between generation and detection functions. Moreover, this overlap slowly disappears as one moves away from the optimized position (± 1 to 2% of relative thickness change). Indeed, as previously said, finite size effects spectrally broaden the two processes. Some non-negligeable overlap is partially assured by the backreflection of the probe beam, since the $q = 0$ mode can be detected when its frequency approximates the one of the same mode of the wedged SL. We checked that mode amplitudes linearly increase with the pump intensity as long

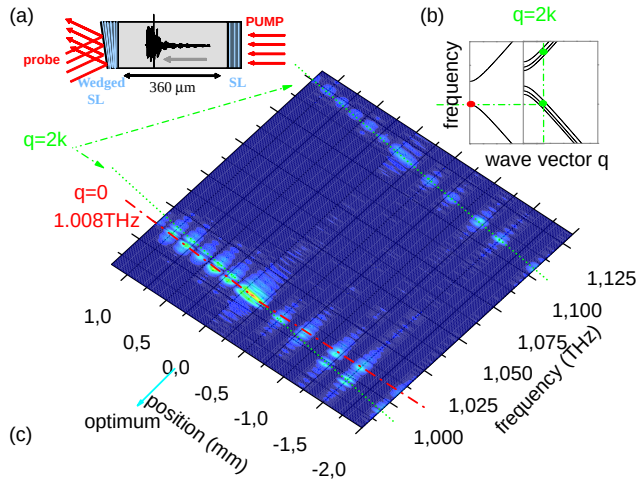

Figure 15: (a) Scheme of the experiment with a SL on one side of the substrate and a tapered SL on the other side, allowing the spectral tuning of the detection response. (b) Matching between generation ($q = 0$ mode) and detection (the gradient of thickness implies a continuous change of the dispersion curve). (c) Fourier transform amplitudes for different positions of the probe on the tapered SL on sample DS1. Dotted lines are guidelines to follow the detected modes (in green) and the generated mode at 1.008 THz (in red). The laser wavelength was $\lambda = 695$ nm.

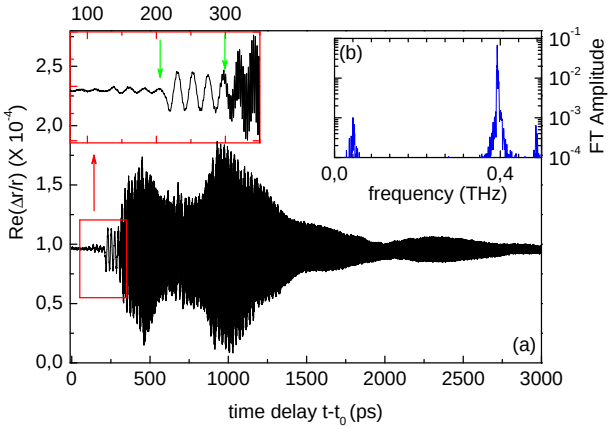

Figure 16: (a) Transient reflectivity for sample DS400, at a pump intensity of 7.9 nJ/pulse and a laser wavelength $\lambda = 769$ nm. Inset : enlargement of the beginning of the signal, where arrows indicate the arrival times of Brillouin and $q = 0$ mode components (≈ 200 and 300 ps respectively). (b) Corresponding FT of the derivative of the time trace: the $q = 0$ mode at 395 GHz dominates by 2 orders of magnitude the $q = 2k$ modes.

as the latter remains lower than 1.2 nJ/pulse. Thus, neglecting nonlinearities during propagation, we could combine the calculations of generation and detection as previously described, and obtain a behaviour in agreement with experimental data, in particular for the gain obtained at the optimal position[67].

From now we will discuss signals obtained on the optimal position on the sample. The figure 16 presents the temporal signal measured at high pump intensity for sample S400. At a wavelength where the detection is very efficient, the signal is dominated by the $q = 0$ mode at 396 GHz, by nearly 2 orders of magnitude. If we focus on the beginning of the signal, we clearly see three regimes. As it has been noticed in the detection configuration (figure 8), the SL is weakly transparent, allowing that a fraction of probe light reaches the substrate and interacts with the incoming acoustic wave. This gives rise to the first Brillouin oscillations seen before $t - t_0 = 200$ ps. The amplitude jump gives an accurate indication of the entering of the acoustic wave in the SL. This wave, generated by the other SL has undergone dispersion during propagation. That explains that the Brillouin component is first detected, corresponding to the second temporal window $200\,\text{ps} < t - t_0 < 300\,\text{ps}$. Then after 300 ps, higher frequency components, *i. e.* $q = 0$ mode at 396 GHz and a small component at 486 GHz ($q = 2k$), are also detected and last for 3000 ps. This duration is explained by the same statements as in § 6.4 where the acoustic wave which is detected has been generated by a SL (duration of $\approx$ 2.25 ns). Indeed, here the SL is 1.25 times thicker so the detection should last longer. In addition, the generated mode is spectrally thinner, as the number of periods has increased by 1.25. For all these reasons, the signal should last more than 1.25 times the duration in the case of S400, *i. e.* 2800 ps. The experimental value ($\approx$ 3200 ps) agrees with these statements.

Calculations give also a good simulation of the signal in the temporal domain, as shown in figure 17. These are results obtained on DS1. The panel (d) from figure 17 shows the spectral features, and here the $q = 0$ mode is not very large compared to the Brillouin component, possibly because the laser wavelength could not be optimized (692 nm is very close to the edge of the laser wavelength operating range). Note that the shape of the signal differs from figure 16 as the pump intensity is very low here. Four discontinuities are now better distinguished at regular intervals corresponding to the travel time within a SL (respectively 237 and 244 ps). The maximum intensity happens at $t_0 + 471$ ps, the travel time through the whole structure (substrate+2SL). The comparison between calculations and the signal, filtered at brillouin and $q = 0$ modes (blue and red respectively) is shown on panels (b) and (c) from figure 17. General features are very well reproduced, including the shape of both signals and the delay undergone by the high frequency. The delay was well adjusted with $\gamma = (6.10 \pm 0.2) \times 10^{-3}$. The same experiments have been performed on similar samples DS400, DS700, DS800, (with two SLs) designed for respective central frequencies 0.395, 0.715, and 0.787 THz. In addition to these 4 samples described in table 1, we include the results obtained on a sample similar to S400, with a thicker substrate (983 μm). The relative time delay for the high frequency is reported on figure 18 and the best fit with the equation 6 gives a value $\gamma = (6.90 \pm 0.1) \times 10^{-3}$, which is slightly smaller than 7.4×10^{-3} nm^3.ps^{-1} from Ref. [39].

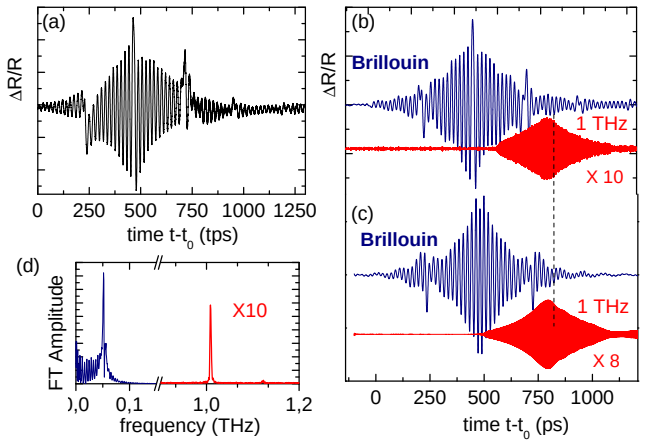

Figure 17: (a) Transient reflectivity for sample DS1, at a pump intensity of 0.7 nJ/pulse and a laser wavelength $\lambda = 693$ nm. (d) Corresponding Fourier transform amplitude (magnified by 10 around 1 THz). (b) 0.01 to 0.08 THz (around Brillouin frequency, in blue) and 0.9 to 1.1 THz (in red) band pass filters of the signal. (c) Same filters on calculated reflectivity. The experimental (calculated) filtered signal at 1 THz has been magnified by 10 (by 8 respectively).

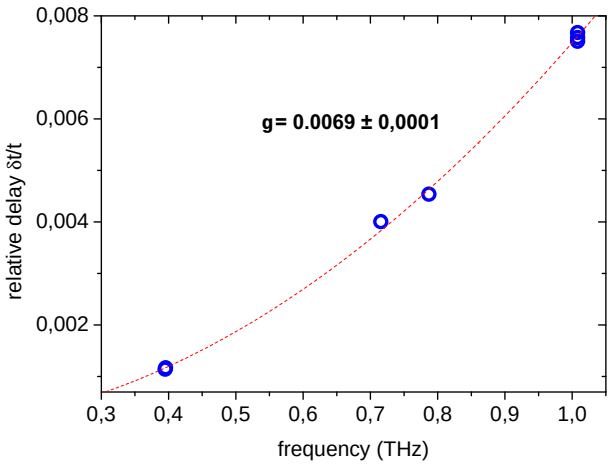

Figure 18: Relative delays obtained for samples DS400, for a sample similar to DS400 but thicker, DS700 DS800 and 3 determinations for DS1, plotted versus the generated wave frequency at $q = 0$. The dotted line is the best fit obtained with the value $\gamma = (6.90 \pm 0.1) \times 10^{-3}$ for the dispersion parameter.

7.2. Efficiency of detection or generation

The gain obtained with such a scheme is demonstrated by the comparison of this experiment and the one where a unique SL detects the phonons it has generated, described in § 6.4. Indeed, in the optimal conditions, *i. e.* with optimization of the position on the sample and of the laser wavelength, the figure 16 shows typical signals in the case of DS400. At a lower pump intensity of 1.65 nJ/pulse where no saturation occurs (peak amplitudes increase linearly with the pump intensity), the peak amplitude at 393 GHz amounts to 0.045. At the same pump intensity and at an optimized laser wavelength (778 nm), the generation and detection by sample S400 only allow a peak detection of 0.0008 at 394 GHz. Of course the fact that sample DS400 has a larger number of periods will induce a correction, but will not affect a lot the measured gain of 56.

Another possible comparison allows to estimate the efficiency of generation by a SL designed to generate at 400 GHz, in comparison with an aluminum film. We have seen, in the case of figure 16 in the optimal conditions, that the SL generates a component at about 400 GHz which amplitude reaches 0.07, measured with another SL. The signal generated by an aluminum film was detected by a similar SL (sample S400) in the "detection configuration" (*cf.* § 6.1). With the same probe wavelength (777 nm) the amplitude at 360 GHz (450 GHz resp.) reaches a value of 0.014 (0.005 resp.), when the pump intensity on aluminum film is quite large (7.9 nJ/pulse). Taking into account the difference of the number of periods, we can conclude that around 400 GHz the aluminum film generates an amplitude smaller by a factor of 4 to 11.

7.3. Optical control

The fact that phonons are coherently excited in these experiments gives the possibility for an optical control using multiple pump pulses. Coherent control experiments have been used to manipulate electronic states, and control the carrier population in nanostructures as quantum wells[68]. They were also realized on LO phonons in bulk semiconductors[69, 70]. Concerning acoustic phonons, coherent control has been performed in semiconductor SLs or nanocavities based on SLs, in classical pump probe experiments directly on the structure[71, 72]. With a second pump pulse with a tunable time delay τ relatively to the first pump pulse, it was possible to extinct excited phonons from the first zone-center gap and enhance the ones from the second gap, or modulate the amplitude of the $q = 0$ mode. At the same time, an enhancement of the purely vibrational response was obtained[73]. In [74] such a double-pump pulse configuration could allow a coherent control of breathing vibrations of silver nanospheres, and the excitation of the first order radial mode usually dominated by the fundamental mode.

The control of the amplitude of the wave packet detected after propagation was perfomed on sample DS400.

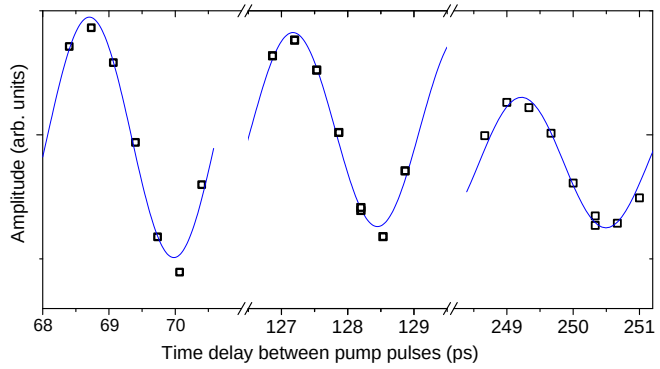

Figure 19: In the double pump pulse experiment, FT amplitude of the peak at 0.393 THz (□) for sample DS400, as the time separating the two pump pulses inscreases. The pump intensity for one pulse is 4.2 nJ/pulse and the laser wavelength is $\lambda = 772$ nm. The line is a guide to the eye for the expected oscillatory behavior.

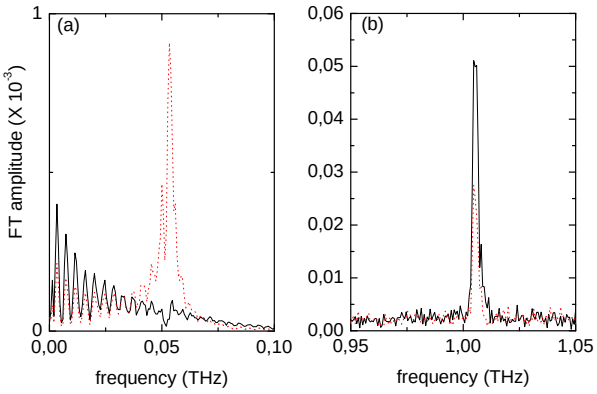

Figure 20: FT amplitude of the derivative of the reflectivity (real part) for sample DS, (a) in the low frequency range and (b) around 1 THz. The dotted line corresponds to the one pump pulse experiment whereas the solid line is the spectrum obtained in the double pump pulse experiment. The pump intensity was 0.2nJ/pulse.

Two optical paths, similar to a Michelson interferometer, are inserted into the pump beam; the mirror of one of the paths is constituted by a prism used as a retroreflector on a mechanical stage. The delay τ is adjusted thanks to the position of this prism. If τ is an odd number of the semi-period of the acoustic phonon wave packet and smaller than the duration of the wave packet, the second pump will generate a wave packet which will interact with the first one destructively. This interference will be efficient if saturation of electronic transitions is avoided. The two pump beams have exactly the same intensity which moreover should influence the acoustic interference contrast. The amplitude of the FT at the $q = 0$ mode is plotted on figure 19 as the delay between the two pump pulses increases. As expected we obtain an oscillatory behavior, with a period invert of the $q = 0$ mode frequency.

At high pump pulse energy, while increasing the time delay between the two pump pulses, we observed that the amplitude of these oscillations decreases and that the extinction of the mode is not perfect. This behavior could be ascribed to saturation effects of the first pulse on phonon generation processes: indeed the contrast varies from 50% (as shown on figure 19) to 80% when the pump pulse energy is decreased by a factor 3.

Coherent control on Brillouin oscillations can also be used to damp the Brillouin oscillations and simultaneously emphasize the high frequency mode. We performed such an experiment on sample DS1 by using 2 pump pulses delayed by one Brillouin half period, namely 19.8 ps in order to generate quite opposite Brillouin oscillations and in phase 1 THz oscillations. In the Fourier transform spectra shown in figure 20(a), a hole appears at the Brillouin frequency, while the 1 THz component is increased by a factor of 2 (*cf.* figure 20(b))

7.4. Applications

This device, presenting two SLs on each side of the substrate, has been used as a sensitive tool for the study of propagation properties of high frequency phonons through the GaAs bulk medium. The relative changes of the amplitude of the quasi monochromatic mode was measured as a function of temperature, and we deduced the varying part of the attenuation by

$$\alpha(T) - \alpha_0 = \ln(\mathrm{A}(T)/\mathrm{A}_0)/L \qquad (7)$$

where L is the substrate thickness, $\mathrm{A}(T)$ and A_0 (respectively $\alpha(T)$ and α_0) the amplitudes of the mode (respectively the attenuation) at the temperature T and at $T \approx 13$ K. The pump intensity was carefully adjusted to avoid saturation. The signal variation with temperature is attributed to phonon scattering in the substrate, mainly due to anharmonic processes which have a significant dependence with temperature. We assume that the efficiency of the generator and the sensitivity of the detector do not vary with temperature, as they are both related to the position of the laser wavelength relatively to that of the SL electronic transition. This assumption is correct since electronic transition energies are nearly constant in the temperature range we explored.

From further experiments we could extrapolate that such experiments could be performed at room temperature with typical propagation distances of 10 μm. A more complete study is the subject of a forthcoming publication.

Conclusion

The principles of terahertz acoustics using superlattices are now well established. The possibility to generate, propagate over large distances and detect monochromatic coherent acoustic waves up to 1 terahertz has been clearly demonstrated and experiments have been performed either after a round trip or a simple transmission through thick wafers. The key point is to use high quality superlattices with a few hundreds nanometric periods. The probe laser wavelength has to be tuned close to an electronic transition of the superlattice in order to maximize the photoelastic coefficients. Optical planar cavities can also be

used to improve the detection sensitivity. These terahertz transducers could be useful for acoustic spectroscopy, measurements of phonon mean free paths or high resolution phonon imaging.

Acknowledgements

This study was supported in part by the ANR Nanosonique ANR-05-NANO-022-01 and SONORE ANR-08-NANO-016.

[1] S. A. Cavill, L. J. Challis, A. J. Kent, F. F. Ouali, A. V. Akimov, M. Henini, Acoustic phonon-assisted tunneling in GaAs/AlAs superlattices, Phys. Rev. B 66 (2002) 235320.
URL http://prb.aps.org/abstract/PRB/v66/i23/e235320

[2] O. L. Muskens, A. V. Akimov, J. I. Dijkhuis, Coherent interactions of terahertz strain solitons and electronic two-level systems in photoexcited ruby, Phys. Rev. Lett. 92 (2004) 035503. doi:10.1103/PhysRevLett.92.035503.
URL http://link.aps.org/doi/10.1103/PhysRevLett.92.035503

[3] D. R. Fowler, a. V. Akimov, a. G. Balanov, M. T. Greenaway, M. Henini, T. M. Fromhold, a. J. Kent, Semiconductor charge transport driven by a picosecond strain pulse, Applied Physics Letters 92 (23) (2008) 232104. doi:10.1063/1.2942389.
URL http://link.aip.org/link/APPLAB/v92/i23/p232104/s1&Agg=doi

[4] C. Bruggeman, A. V. Akimov, A. V. Scherbakov, M. Bombeck, C. Schneider, S. Ho, A. Forchel, D. R. Yakovlev, M. Bayer, Laser mode feeding by shaking quantum dots in a planar microcavity, Nature Photonics (November) (2011) 1–5. doi:10.1038/nphoton.2011.269.
URL http://www.nature.com/nphoton/journal/vaop/ncurrent/full/nphoton.2011.269.html#/main

[5] R. J. V. Gutfeld, A. H. Nethercot, Phys. Rev. Lett. 12 (1964) 641.

[6] M. Terraneo, M. Peyrard, G. Casati, Controlling the energy flow in non-linear lattices: A model for a thermal rectifier, Phys. Rev. Lett. 88 (2002) 094302. doi:10.1103/PhysRevLett.88.094302.
URL http://link.aps.org/doi/10.1103/PhysRevLett.88.094302

[7] B. Li, L. Wang, G. Casati, Thermal diode: Rectification of heat flux, Phys. Rev. Lett. 93 (2004) 184301. doi:10.1103/PhysRevLett.93.184301.
URL http://link.aps.org/doi/10.1103/PhysRevLett.93.184301

[8] B. Li, J. Lan, L. Wang, Interface thermal resistance between dissimilar anharmonic lattices, Phys. Rev. Lett. 95 (2005) 104302. doi:10.1103/PhysRevLett.95.104302.
URL http://link.aps.org/doi/10.1103/PhysRevLett.95.104302

[9] D. Segal, A. Nitzan, Spin-boson thermal rectifier, Phys. Rev. Lett. 94 (2005) 034301. doi:10.1103/PhysRevLett.94.034301.
URL http://link.aps.org/doi/10.1103/PhysRevLett.94.034301

[10] B. Hu, L. Yang, Y. Zhang, Asymmetric heat conduction in nonlinear lattices, Phys. Rev. Lett. 97 (2006) 124302. doi:10.1103/PhysRevLett.97.124302.
URL http://link.aps.org/doi/10.1103/PhysRevLett.97.124302

[11] D. Segal, Single mode heat rectifier: Controlling energy flow between electronic conductors, Phys. Rev. Lett. 100 (2008) 105901. doi:10.1103/PhysRevLett.100.105901.
URL http://link.aps.org/doi/10.1103/PhysRevLett.100.105901

[12] B. Li, L. Wang, G. Casati, Negative differential thermal resistance and thermal transistor, Applied Physics Letters 88 (14) (2006) 143501. doi:10.1063/1.2191730.
URL http://scitation.aip.org/content/aip/journal/apl/88/14/10.1063/1.2191730

[13] L. Wang, B. Li, Thermal logic gates: Computation with phonons, Phys. Rev. Lett. 99 (2007) 177208. doi:10.1103/PhysRevLett.99.177208.
URL http://link.aps.org/doi/10.1103/PhysRevLett.99.177208

[14] C. Thomsen, H. T. Grahn, H. J. Maris, T. Tauc, Surface generation and detection of phonons by picosecond light pulses, Phys. Rev. B 34 (1986) 4129.

[15] J. Baumberg, D. Williams, K. Köhler, Ultrafast Acoustic Phonon Ballistics in Semiconductor Heterostructures, Physical Review Letters 78 (17) (1997) 3358–3361. doi:10.1103/PhysRevLett.78.3358.
URL http://link.aps.org/doi/10.1103/PhysRevLett.78.3358

[16] C. Colvard, R. Merlin, M. V. KLein, Observation of folded acoustic phonons in a semiconductor superlattice, Phys. Rev. Lett. 45 (4) (1980) 298–301.

[17] C. Colvard, T. A. Gant, M. V. Klein, R. Merlin, R. Fischer, H. Morkoc, A. C. Gossard, Folded acoustic and quantized optic phonons in (gaal)as superlattices, Phys. Rev. B 31 (1985) 2080–2091. doi:10.1103/PhysRevB.31.2080.
URL http://link.aps.org/doi/10.1103/PhysRevB.31.2080

[18] P. Santos, M. Hundhausen, L. Ley, Observation of zone-folded acoustical phonons by Raman scattering in amorphous Si-SiNx superlattices, Phys. Rev. B 33 (2) (1986) 1516–1518.

[19] B. Jusserand, D. Paquet, F. Mollot, F. Alexandre, G. Le Roux, Influence of the supercell structure on the folded acoustical raman line intensities in superlattices, Phys. Rev. B 35 (1987) 2808–2817. doi:10.1103/PhysRevB.35.2808.
URL http://link.aps.org/doi/10.1103/PhysRevB.35.2808

[20] V. Narayanamurti, H. L. Störmer, M. A. Chin, A. C. Gossard, W. Wiegmann, Selective transmission of high-frequency phonons by a superlattice: The "dielectric" phonon filter, Phys. Rev. Lett. 43 (1979) 2012–2016. doi:10.1103/PhysRevLett.43.2012.
URL http://link.aps.org/doi/10.1103/PhysRevLett.43.2012

[21] H. T. Grahn, H. J. Maris, J. Tauc, B. Abeles, Phys. Rev. B 38 (1988) 6066.

[22] P. Basséras, S. M. Gracewski, G. W. Wicks, R. J. D. Miller, J. Appl. Phys. 75 (1994) 2762.

[23] A. Yamamoto, T. Mishina, Y. Masumoto, M. Nakayama, Coherent oscillation of zone-folded phonon modes in gaas-alas superlattices, Phys. Rev. Lett. 73 (1994) 740–743. doi:10.1103/PhysRevLett.73.740.
URL http://link.aps.org/doi/10.1103/PhysRevLett.73.740

[24] A. Bartels, T. Dekorsy, H. Kurz, K. Köhler, Coherent zone-folded longitudinal acoustic phonons in semiconductor superlattices: Excitation and detection, Phys. Rev. Lett. 82 (1999) 1044–1047.

[25] K. Mizoguchi, M. Hase, S. Nakashima, M. Nakayama, Observation of coherent folded acoustic phonons propagating in a gaas/alas superlattice by two-color pump-probe spectroscopy, Phys. Rev. B 60 (1999) 8262.

[26] W. Chen, Y. Lu, H. J. Maris, G. Xiao, Phys. Rev. B 50 (1994) 14506.

[27] B. Perrin, B. Bonello, J.-C. Jeannet, E. Romatet, Physica B 219-220 (1996) 681.

[28] C. Rossignol, B. Perrin, Picosecond ultrasonics study of periodic multilayers, analytical sciences 17 (2001) 245.

[29] N.-W. Pu, Ultrafast excitation and detection of acoustic phonon modes in superlattices, Physical Review B 72 (2005) 115428.

[30] L. Belliard, A. Huynh, B. Perrin, A. Michel, G. Abadias, C. Jaouen, Elastic properties and phonon generation in mo/si superlattices, Phys. Rev. B 80 (2009) 155424.

[31] P. Hawker, A. J. Kent, L. J. Challis, A. Bartels, T. Dekorsy, H. Kurz, Appl. Phys. Lett. 77 (2000) 3209.

[32] N. M. Stanton, R. N. Kini, A. J. Kent, M. Hinini, D. Lehmann, Phys. Rev. B 68 (2003) 113302.

[33] W. M. Robertson, C. Baker, C. B. Bennett, Slow group velocity propagation of sound via defect coupling in a one-dimensional acoustic band gap array, American Journal of Physics 72 (2) (2004) 255. doi:10.1119/1.1596192.
URL http://link.aip.org/link/AJPIAS/v72/i2/p255/s1&Agg=doi

[34] F. Montero de Espinosa, E. Jiménez, M. Torres, Ultrasonic Band Gap in a Periodic Two-Dimensional Composite, Physical Review Letters 80 (6) (1998) 1208–1211. doi:10.1103/PhysRevLett.80.1208.
URL http://link.aps.org/doi/10.1103/PhysRevLett.80.1208

[35] S. Yang, J. Page, Z. Liu, M. Cowan, C. Chan, P. Sheng, Ultrasound Tunneling through 3D Phononic Crys-

tals, Physical Review Letters 88 (10) (2002) 104301. doi:10.1103/PhysRevLett.88.104301.
URL http://link.aps.org/doi/10.1103/PhysRevLett.88.104301
[36] P. V. Santos, L. Ley, J. Mebert, O. Koblinger, Frequency gaps for acoustic phonons in a-Si:H/a-SiNx:H superlattices, Physical Review B 36 (1987) 4858–4867. doi:10.1103/PhysRevB.36.4858.
URL http://link.aps.org/doi/10.1103/PhysRevB.36.4858
[37] J.-Y. Duquesne, B. Perrin, Phys. Rev. B 68 (2003) 134205.
[38] H. Maris, Picosecond Ultrasonics, Scientific American 278 (1998) 86–89. doi:10.1038/scientificamerican0198-86.
[39] H.-Y. Hao, H. J. Maris, Experiments with acoustic solitons in crystalline solids, Phys. Rev. B 64 (2001) 64302.
[40] E. Peronne, B. Perrin, Generation and detection of acoustic solitons in crystalline slabs by laser ultrasonics, Ultrasonics 44 (2006) 1203.
[41] P. a. Elzinga, R. J. Kneisler, F. E. Lytle, Y. Jiang, G. B. King, N. M. Laurendeau, Pump/probe method for fast analysis of visible spectral signatures utilizing asynchronous optical sampling., Applied optics 26 (19) (1987) 4303–9.
URL http://www.ncbi.nlm.nih.gov/pubmed/20490226
[42] C. Janke, M. Först, M. Nagel, H. Kurz, a. Bartels, Asynchronous optical sampling for high-speed characterization of integrated resonant terahertz sensors., Optics letters 30 (11) (2005) 1405–7.
URL http://www.ncbi.nlm.nih.gov/pubmed/15981548
[43] A. Bartels, F. Hudert, C. Janke, T. Dekorsy, K. Köhler, Femtosecond time-resolved optical pump-probe spectroscopy at kilohertz-scan-rates over nanosecond-time-delays without mechanical delay line, Applied Physics Letters 88 (4) (2006) 041117. doi:10.1063/1.2167812.
URL http://scitation.aip.org/content/aip/journal/apl/88/4/10.1063/1.2167812
[44] B. Perrin, B. Bonello, J. C. Jeannet, E. Romatet, Interferometic detection of hypersound waves in modulated structures, Prog. Nat. Sci. 6 (1996) 444.
[45] G. Tas, H. Maris, Electron diffusion in metals studied by picosecond ultrasonics, Physical Review B 49 (21) (1994) 46–54.
URL http://prb.aps.org/abstract/PRB/v49/i21/p15046_1
[46] O. B. Wright, V. E. Gusev, Ultrafast generation of acoustic waves in copper, IEEE Transactions on Ulrasonics, Ferroelectrics, and Frequency Control 42 (1995) 331–338. doi:10.1109/58.384440.
[47] O. Muskens, A. V. Akimov, J. I. Dijkhuis, Coherent interactions of terahertz strain solitons and electronic two-level systems in photoexcited ruby, Phys. Rev. Lett. 92 (2004) 35503.
[48] T. a. Driscoll, A Composite Runge?Kutta Method for the Spectral Solution of Semilinear PDEs, Journal of Computational Physics 182 (2) (2002) 357–367. doi:10.1006/jcph.2002.7127.
URL http://linkinghub.elsevier.com/retrieve/pii/S0021999102971277
[49] C. Thomsen, J. Strait, Z. Vardeny, H. J. Maris, J. Tauc, J. J. Hauser, Coherent phonon generation and detection by picosecond light pulses, Phys. Rev. Lett. 53 (1984) 989–992. doi:10.1103/PhysRevLett.53.989.
URL http://link.aps.org/doi/10.1103/PhysRevLett.53.989
[50] M. Trigo, A. Bruchhausen, A. Fainstein, B. Jusserand, V. Thierry-Mieg, Confinement of acoustical vibrations in a semiconductor planar phonon cavity, Phys. Rev. Lett. 89 (2002) 227402.
[51] A. Huynh, N. D. Lanzillotti-Kimura, B. Jusserand, B. Perrin, A. Fainstein, M. F. Pascual-Winter, E. Peronne, A. Lemaître, Phys. Rev. Lett. 97 (2006) 115502.
[52] A. Fainstein, N. D. Lanzillotti-Kimura, B. Jusserand, B. Perrin, Strong optical-mechanical coupling in a vertical gaas/alas microcavity for subterahertz phonons and near-infrared light, Phys. Rev. Lett. 110 (2013) 037403. doi:10.1103/PhysRevLett.110.037403.
URL http://link.aps.org/doi/10.1103/PhysRevLett.110.037403
[53] W. Maryam, a. V. Akimov, R. P. Campion, a. J. Kent, Dynamics of a vertical cavity quantum cascade phonon laser structure., Nature communications 4 (2013) 2184. doi:10.1038/ncomms3184.
URL http://www.pubmedcentral.nih.gov/articlerender.fcgi?artid=3731554&tool=pmcentrez&rendertype=abstract
[54] A. Huynh, B. Perrin, N. D. Lanzillotti-Kimura, B. Jusserand, A. Fainstein, A. Lemaître, Phys. Rev. B 78 (2008) 233302.
[55] B. Perrin, Systèmes femtosecondes, Publication de l'Université de Saint-Etienne, 2000.
[56] O. B. Wright, B. Perrin, O. Matsuda, V. E. Gusev, Ultrafast carrier diffusion in gallium arsenide probed with picosecond acoustic pulses, Phys. Rev. B 64 (2001) 081202(R).
[57] C.-K. Sun, J.-C. Liang, X.-Y. Yu, Coherent acoustic phonon oscillations in semiconductor multiple quantum wells with piezoelectric fields, Phys. Rev. Lett. 84 (2000) 179–182.
[58] C.-Y. Chen, Y.-C. Wen, H.-P. Chen, T.-M. Liu, C.-C. Pan, J.-I. Chyi, C.-K. Sun, Narrow-band detection of propagating coherent acoustic phonons in piezoelectric InGaN?GaN multiple-quantum wells, Applied Physics Letters 91 (13) (2007) 133101. doi:10.1063/1.2785126.
URL http://link.aip.org/link/APPLAB/v91/i13/p133101/s1&Agg=doi
[59] R. Merlin, Generating coherent THz phonons with light pulses, Solid State Communications 102 (2) (1997) 207–220.
URL http://www.sciencedirect.com/science/article/pii/S003810989
[60] P. J. S. van Capel, J. I. Dijkhuis, Erratum: ?Optical generation and detection of shock waves in sapphire at room temperature? [Appl. Phys. Lett. 88, 151910 (2006)], Applied Physics Letters 89 (13) (2006) 139903. doi:10.1063/1.2358196.
URL http://link.aip.org/link/APPLAB/v89/i13/p139903/s1&Agg=doi
[61] P. Hawker, A. Kent, L. Challis, Observation of coherent zone-folded acoustic phonons generated by Raman scattering in a superlattice, Applied Physics Letters 77 (20) (2000) 3209–3211.
URL http://ieeexplore.ieee.org/xpls/abs_all.jsp?arnumber=490503
[62] A. Devos, A. Le Louarn, Strong effect of interband transitions in the picosecond ultrasonics response of metallic thin films, Phys. Rev. B 68 (2003) 045405. doi:10.1103/PhysRevB.68.045405.
URL http://link.aps.org/doi/10.1103/PhysRevB.68.045405
[63] P. J. S. van Capel, J. I. Dijkhuis, Optical generation and detection of shock waves in sapphire at room temperature, Applied Physics Letters 88 (15) (2006) 151910. doi:10.1063/1.2195098.
URL http://link.aip.org/link/APPLAB/v88/i15/p151910/s1&Agg=doi
[64] Y.-C. Wen, C.-L. Hsieh, K.-H. Lin, H.-P. Chen, S.-C. Chin, C.-L. Hsiao, Y.-T. Lin, C.-S. Chang, Y.-C. Chang, L.-W. Tu, C.-K. Sun, Specular Scattering Probability of Acoustic Phonons in Atomically Flat Interfaces, Physical Review Letters 103 (26) (2009) 1–4. doi:10.1103/PhysRevLett.103.264301.
URL http://link.aps.org/doi/10.1103/PhysRevLett.103.264301
[65] M. Trigo, T. A. Eckhause, J. K. Wahlstrand, R. Merlin, M. Reason, R. S. Goldman, Ultrafast optical generation and remote detection of terahertz sound using semiconductor superlattices, Applied Physics Letters 91 (2) (2007) 023115. doi:10.1063/1.2754353.
URL http://scitation.aip.org/content/aip/journal/apl/91/2/10.10
[66] M. F. P. Winter, A. Fainstein, B. Jusserand, B. Perrin, A. Lemaître, Appl. Phys. Lett. 94 (2009) 103103.
[67] A. Huynh, B. Perrin, B. Jusserand, A. Lemaître, Terahertz coherent acoustic experiments with semiconductor superlattices, Applied Physical Letters 99 (2011) 191908.
[68] A. P. Heberle, J. J. Baumberg, K. Köhler, Ultrafast coherent control and destruction of excitons in quantum wells, Phys. Rev. Lett. 75 (1995) 2598–2601. doi:10.1103/PhysRevLett.75.2598.
URL http://link.aps.org/doi/10.1103/PhysRevLett.75.2598
[69] T. Dekorsky, W. Kütt, T. Pfeifer, H. Kurz, Coherent control of LO-phonon dynamics in opaque semiconductors by femtosecond laser pulses, EPL (Europhysics Letters) 23 (1993) 223.
URL http://iopscience.iop.org/0295-5075/23/3/011
[70] M. Hase, K. Mizoguchi, H. Harima, S. Nakashima, M. Tani, K. Sakai, M. Hangyo, Optical control of coherent optical phonons in bismuth films, Applied Physics Letters 69 (17) (1996) 2474–2476. doi:http://dx.doi.org/10.1063/1.117502.
URL http://scitation.aip.org/content/aip/journal/apl/69/17/10.1
[71] A. Bartels, T. Dekorsy, H. Kurz, K. Ko, Coherent control of acoustic phonons in semiconductor superlattices, Applied Physics Letters 72 (22) (1998) 2844–2846.
[72] N. D. Lanzillotti-Kimura, a. Fainstein, a. Lemaitre, B. Perrin, B. Jusserand, Coherent generation and detection of tunable ultrafast sub-terahertz con-

fined acoustic nanowaves: Theory and experiments, Physical Review B 84 (11) (2011) 1–6. doi:10.1103/PhysRevB.84.115453.
URL http://link.aps.org/doi/10.1103/PhysRevB.84.115453

[73] N.-W. Pu, J. Bokor, S. Jeong, R.-A. Zhao, Ultrafast excitation and detection of acoustic phonon modes in superlattices, Applied Physics Letters 74 (1999) 115428. doi:http://dx.doi.org/10.1063/1.123010.

[74] A. Arbouet, N. Del Fatti, F. Vallee, Optical control of the coherent acoustic vibration of metal nanoparticles, The Journal of Chemical Physics 124 (14) (2006) –. doi:http://dx.doi.org/10.1063/1.2185631.
URL http://scitation.aip.org/content/aip/journal/jcp/124/14/10.1063/1.2185631

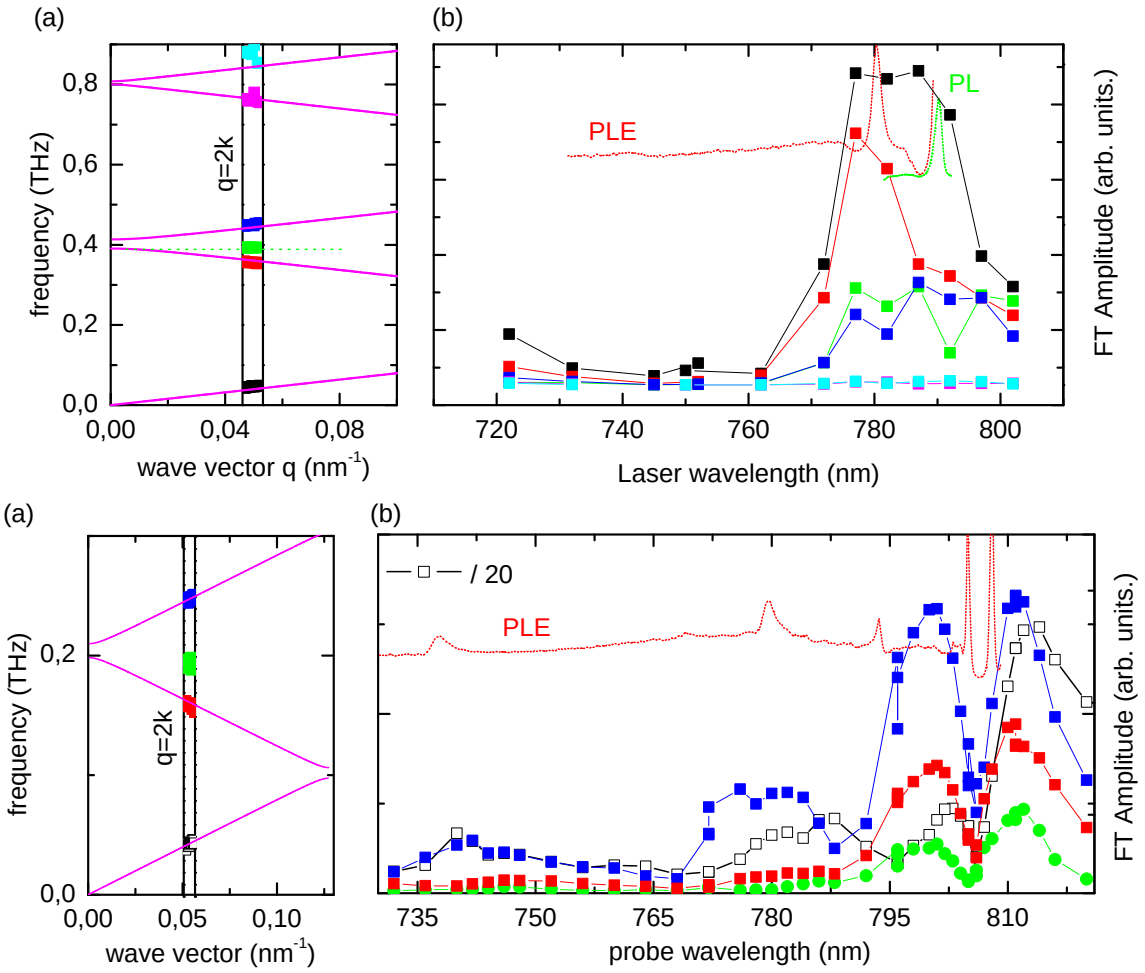

Figure 13: In the detection configuration, for sample S400 (up) and S200 with ASOPS (bottom) with constant pump intensity (8.75 nJ/pulse (S400) or 8 nJ/pulse (S200)) (a) dispersion curve where the detected frequencies (■) are plotted as the laser wavelength varies, resulting in a slight change of the selection rule $q = 2k$. $q = 0$ mode is detected as well. (b) Corresponding FT amplitude at these frequencies as a function of the (probe) laser wavelength. The photoluminescence (PL) and excitation of the photoluminescence (PLE) are plotted as well. The pump wavelength was 750 nm in ASOPS (S200).